

RAPT: Model-Predictive Out-of-Distribution Detection and Failure Diagnosis for Sim-to-Real Humanoid Robots

Humphrey Munn^{1,2}, Brendan Tidd², Peter Böhm^{1,2}, Marcus Gallagher¹, David Howard²

¹School of Electrical Engineering and Computer Science, University of Queensland, QLD 4072, Australia

²CSIRO Robotics, Data61, Australia

Corresponding author: h.munn@uq.edu.au

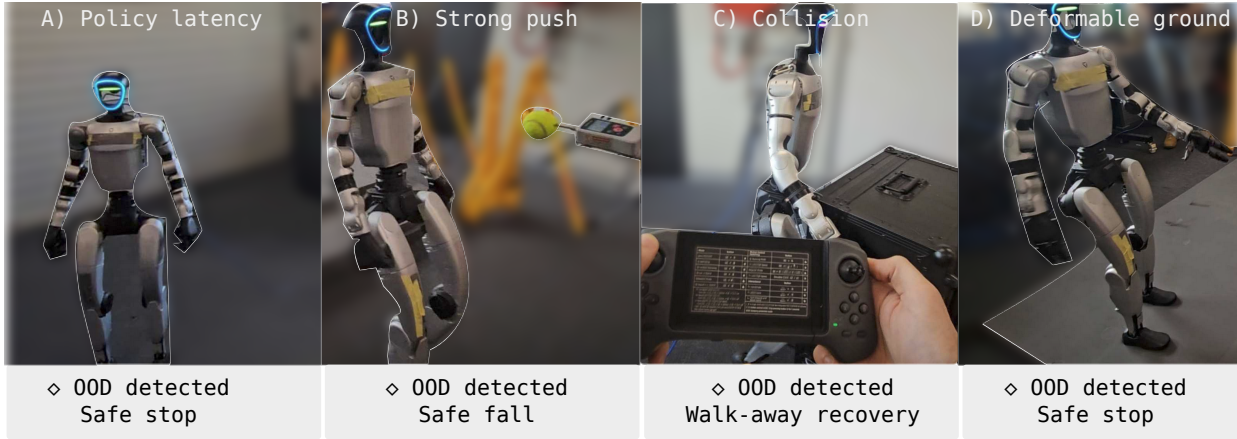


Fig. 1: **RAPT overview.** Real-world out-of-distribution (OOD) scenarios during humanoid deployment. RAPT detects anomalies online and triggers predefined safety responses, including safe stopping, controlled falling, and recovery behaviors.

Abstract—Deploying learned control policies on humanoid robots is challenging: policies that appear robust in simulation can execute confidently in out-of-distribution (OOD) states after Sim-to-Real transfer, leading to silent failures that risk hardware damage. Although anomaly detection can mitigate these failures, prior methods are often incompatible with high-rate control, poorly calibrated at the extremely low false-positive rates required for practical deployment, or operate as black boxes that provide a binary *stop* signal without explaining *why* the robot drifted from nominal behavior. We present RAPT (Recurrent Anomaly Probabilistic Trajectory Model), a lightweight, self-supervised deployment-time monitor for 50 Hz humanoid control. RAPT learns a probabilistic spatio-temporal manifold of nominal execution from simulation and evaluates execution-time predictive deviation as a *calibrated, per-dimension* signal. This yields (i) reliable online OOD detection under strict false-positive constraints and (ii) a continuous, interpretable measure of Sim-to-Real mismatch that can be tracked over time to quantify *how far* deployment has drifted from training. Beyond detection, we introduce an automated post-hoc root-cause analysis pipeline that combines gradient-based temporal saliency derived from RAPT’s reconstruction objective with LLM-based reasoning conditioned on saliency and joint kinematics to produce semantic failure diagnoses in a zero-shot setting. We evaluate RAPT on a Unitree G1 humanoid across four complex tasks in NVIDIA Isaac Lab and on physical hardware. In large-scale simulation, RAPT improves True Positive Rate (TPR) by 37% over the strongest baseline

at a fixed episode-level false positive rate of 0.5%. On real-world deployments, RAPT achieves a 12.5% TPR improvement and provides actionable interpretability, reaching 75% root-cause classification accuracy across 16 real-world failures using only proprioceptive data.

I. INTRODUCTION

The deployment of Deep Reinforcement Learning (DRL) policies in the physical world presents a paradox: while agents demonstrate superhuman performance in controlled simulation environments, their reliability often degrades catastrophically when facing the stochasticity of the real world [14, 9].

Standard DRL algorithms operate under the assumption that test data follows the same distribution as training data, an assumption that rarely holds in open-context deployment [14]. When agents encounter Out-Of-Distribution (OOD) states caused by unmodeled dynamics, sensor noise, or environmental shifts, they typically fail silently, producing high-confidence actions that can lead to hazardous behaviors rather than signaling uncertainty [9, 8]. This *silent failure* mode is particularly dangerous in safety-critical domains such as humanoid deployment, autonomous driving, and healthcare, where irrational outputs can result in significant hardware damage or risk to human operators [14, 12]. Figure 1 illustrates

representative real-world OOD scenarios encountered during humanoid deployment, along with the corresponding safety responses triggered by RAPT.

The urgency of this problem is underscored by the reality of the Sim-to-Real gap, where subtle discrepancies between physics engines and physical hardware manifest as severe OOD events [22]. A motivating example from our own laboratory involved a trained humanoid policy that, upon encountering an unmodeled payload distribution, executed a high-velocity maneuver resulting in a near-miss self-collision. Such incidents reveal that safety in robotic learning requires more than just high task performance; it demands a robust mechanism to detect when the agent has drifted from its training distribution and, crucially, to understand *why* that drift occurred and *how far* the robot has drifted.

Despite the critical need for reliability, existing anomaly detection methods often fall short of the rigorous demands of high-frequency humanoid control. Generative approaches, particularly LSTM-based Variational Autoencoders (VAEs), remain a dominant paradigm for robotic time-series anomaly detection [21]. However, VAEs frequently suffer from *input complexity bias*, a phenomenon where models assign higher likelihoods to OOD inputs than to the training data due to background statistics, rather than semantic relevance [18].

Furthermore, general time-series methods [24, 27] frequently overlook the rigid-body constraints inherent in legged systems. By treating joint sensors as generic, independent signal channels, these approaches fail to model the strict mechanical couplings and non-linear dependencies between joint states and base dynamics that define valid locomotion. Prior works in legged locomotion fault detection have similarly suffered from this limitation, often relying on hand-crafted features or treating proprioceptive sensors in isolation rather than as a coupled kinematic chain [10, 6]. To bridge this gap, effective detection in high-dimensional humanoid control requires dense encoding strategies capable of explicitly capturing the holistic spatio-temporal manifold of the robot.

Most critically, current safety shields generally function as opaque *black boxes*, providing binary stop signals without offering the diagnostic interpretability required to close the Sim-to-Real gap.

In this work, we introduce **RAPT** (Recurrent Anomaly Probabilistic Trajectory Model), a lightweight, deployment-time monitoring and diagnostic system for humanoid robots. RAPT operates alongside a pre-trained control policy and models nominal spatio-temporal behavior to detect deviations during execution. Rather than attempting to eliminate sim-to-real mismatch via domain randomization or system identification, RAPT treats domain shift as an observable deployment-time signal, enabling reliable detection and post-hoc diagnosis of anomalous behavior under strict false-positive constraints.

Our primary contributions are three-fold:

- **Deployment-Time Measurement of Sim-to-Real Gap:**

We re-frame reconstruction likelihood as a calibrated, continuous measure of sim-to-real mismatch during deployment, treating domain shift as an observable signal

rather than a binary outcome, enabling fine-grained monitoring, verification, and debugging beyond success-based metrics.

- **Online, Lightweight OOD Detection for Humanoids:**

We introduce RAPT, a recurrent probabilistic model for high-frequency (50 Hz) detection of out-of-distribution behavior during humanoid deployment. RAPT is designed to be lightweight, fast to train, and deployable, and consistently outperforms prior methods across locomotion, manipulation, and mimicry tasks on the Unitree G1.

- **Saliency-Based Failure Diagnosis:**

We propose a post-hoc diagnostic pipeline that traces reconstruction sensitivity through time and maps gradient-based saliency patterns to semantically meaningful failure descriptions. By combining these structured cues with a multi-modal language model, the system enables zero-shot classification of failure modes, facilitating rapid interpretation of hardware and software faults.

We validate our approach through extensive experimentation in NVIDIA Isaac Lab and on physical hardware. To support the community, we provide our full training pipeline, real-world labeled datasets (nominal and OOD), and C++ deployment code in the supplementary material.

II. RELATED WORK

We organize prior work by the signals and modeling assumptions used to monitor, detect, and interpret distributional shift during RL deployment. OOD detection in RL remains fragmented in terminology and benchmarks [22, 19]; unlike supervised learning, anomalies may arise from sensory corruptions (covariate shift) or changes in environment dynamics (semantic shift) [8, 19]. Below we group methods by their primary detection mechanism.

A. Uncertainty Estimation and Ensembles

Uncertainty-based methods assume epistemic uncertainty increases in sparsely visited regions of the state-action space [19]. MC Dropout/DropConnect approximate Bayesian inference by performing multiple stochastic forward passes at inference time [14], but often conflate aleatoric and epistemic uncertainty [22]. While simple to implement, these methods incur inference-time costs that scale linearly with the number of samples. Ensembles typically improve detection via disagreement [14], yet are mainly sensitive to unfamiliar *states* and may miss *environment* shifts (e.g., altered transition dynamics) when the policy remains confidently wrong [22]. Furthermore, ensemble methods impose substantial computational and memory overhead at inference, scaling poorly with model size, limiting applicability in real-time deployment. Finally, these methods do not naturally support gradient-based saliency or attribution, limiting their usefulness for diagnosing the underlying causes of sim-to-real failures. In contrast, our approach produces a single-pass, per-dimension anomaly signal that supports both real-time detection and post-hoc interpretability.

B. Generative and Reconstruction-Based Methods

Density and reconstruction approaches model in-distribution observations and flag low likelihood or high reconstruction error. VAEs (including LSTM-based variants) have been used to detect anomalies in multimodal robotic streams, often with phase-dependent thresholds [21]. A key limitation is *input complexity bias*: deep generative models can assign higher likelihood to certain OOD inputs than to complex in-distribution data [18], undermining naive likelihood thresholds.

In contrast, while our method is also reconstruction-based, it differs in how reconstruction error is structured and used: predictive deviations are evaluated probabilistically, decomposed per dimension, and calibrated relative to nominal behavior over time, enabling robust detection under strict false-positive constraints and supporting interpretable diagnosis.

C. Dynamics Modeling and Transition Estimation

To capture semantic shifts, dynamics-based methods model MDP transitions (e.g., $P(s_{t+1} | s_t, a_t)$) and detect deviations between predicted and observed transitions. Probabilistic ensemble dynamics models (PEDM) show robustness under severe mechanical perturbations [8]. Related work uses CVAEs to approximate transition kernels and conformal prediction to provide statistical detection guarantees [22]. These approaches can be computationally heavy and may struggle with *silent failures* where transitions remain consistent but observations are temporally corrupted [19].

While our model may condition on actions for certain tasks (e.g., walking), it is not trained as an explicit dynamics model of the environment. Instead, it learns a compressed representation of nominal spatio-temporal behavior, using predictive error as a calibrated consistency signal rather than a measure of transition accuracy.

D. Temporal and Time-Series Analysis

Many real-world failures are temporally correlated (e.g., drift or persistent occlusions), which step-wise detectors can miss [19]. Time-series methods address this by extracting temporal features or accumulating evidence over time (e.g., via sequential tests) to detect subtle, persistent shifts [19]. However, most generic pipelines treat channels independently, neglecting kinematic couplings and rigid-body constraints.

E. Control Theoretic Safety and Constraints

Control-theoretic safety methods provide verifiable constraint satisfaction (often framed as Level-III safety) via Lyapunov analysis, CBFs, and constrained MPC/shielding [3, 2, 5, 4, 1, 11, 20]. Their practicality is limited by dependence on accurate explicit dynamics and the intractability of formal guarantees in high-dimensional, unstructured observation spaces typical of deep RL [9, 17]. In contrast, RAPT is designed for high-dimensional latent spaces where explicit equations of motion are unavailable, addressing the gap where traditional model-based guarantees cannot be applied.

A key limitation of many OOD methods is interpretability: detection alone is insufficient for debugging sim-to-real

failures. Our approach addresses this by combining anomaly signals with gradient-based saliency, enabling post-hoc attribution of failures to underlying physical or sensing factors.

Overall, prior OOD approaches emphasize uncertainty estimation, dynamics modeling, or generic time-series analysis, whereas our method treats predictive deviation as an interpretable deployment-time signal for detection and diagnosis.

III. METHODOLOGY

Our approach consists of four stages: (i) collecting nominal execution data from expert policies in simulation; (ii) training a probabilistic, self-supervised detector on this data; (iii) performing real-time out-of-distribution detection during deployment; and (iv) post-hoc root-cause diagnosis using loss-based saliency and an LLM-based diagnostic agent. The full pipeline can be trained in under 15 minutes on consumer-grade hardware, enabling rapid iteration during sim-to-real deployment. Figure 2 summarizes the full pipeline.

A. Experimental Tasks & Data Collection

We evaluate our method across four humanoid control tasks on the Unitree G1 robot (29 DoF) in both simulation and real-world experiments. For each task, nominal training data is collected by executing a pre-trained expert policy in large-scale simulation, yielding a dataset of proprioceptive observations $\mathbf{o}_t \in \mathbb{R}^{d_{obs}}$ representative of normal task execution. All observations are normalized to zero mean and unit variance prior to training the corresponding RAPT model.

B. RAPT Architecture and Training

RAPT is a self-supervised reconstruction model trained on nominal execution data to capture characteristic temporal structure in robot behavior. Deviations from this learned structure are expected to produce elevated reconstruction error at deployment. The architecture consists of a residual state encoder, a GRU-based latent bridge, and a probabilistic decoder producing per-dimension likelihoods.

1) *Residual State Encoder*: The encoder projects the observation \mathbf{o}_t into a higher-dimensional latent embedding \mathbf{e}_t ($d_{model} > d_{obs}$). This expansion provides sufficient capacity to capture non-linear kinematic couplings across the robot's degrees of freedom, facilitating subsequent temporal modeling. The encoder f_ϕ is a Multi-Layer Perceptron (MLP) with an initial projection to $d_{model} = 256$, followed by $L = 4$ residual blocks:

$$\mathbf{e}_t = f_\phi(\mathbf{o}_t) \in \mathbb{R}^{256}. \quad (1)$$

Each residual block operates on an intermediate representation \mathbf{x}_l and applies a non-linear transformation with a skip connection to improve optimization stability:

$$\mathbf{x}_{l+1} = \sigma(\text{LN}(\mathbf{x}_l + \mathcal{F}(\mathbf{x}_l))), \quad (2)$$

where $\mathcal{F}(\cdot)$ denotes a linear layer, LN denotes Layer Normalization, and σ is the ReLU activation function.

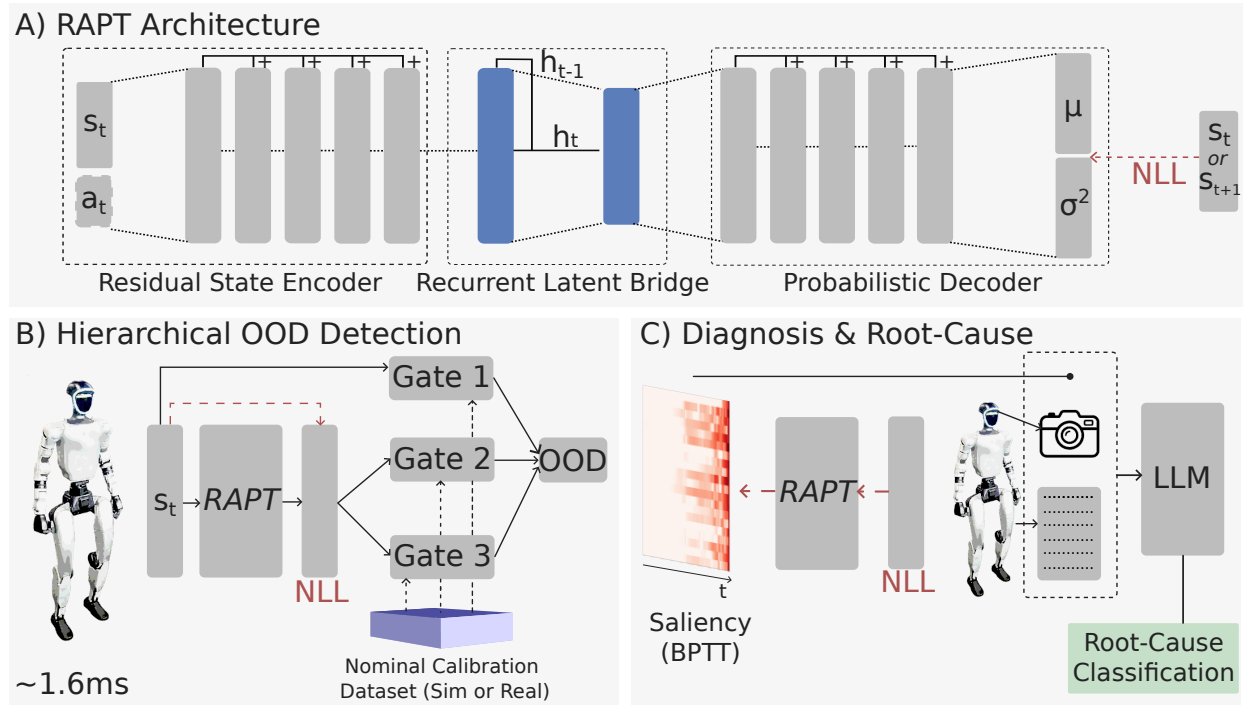


Fig. 2: **RAPT Method Overview:** (A) RAPT OOD-detection architecture. (B) Hierarchical OOD pipeline using three statistical gates for real-time ($\sim 1.6\text{ms}$) monitoring. (C) Detected anomalies trigger gradient-based saliency generation (s_t) for zero-shot diagnosis via a multi-modal LLM.

2) *Recurrent Latent Bridge*: While individual states may appear nominal, anomalies often manifest through inconsistent temporal evolution. To capture such effects, we introduce a Gated Recurrent Unit (GRU) operating in the latent space. Following prior world-modeling approaches [7], temporal dependencies are modeled over compact latent embeddings rather than raw observations, enabling efficient aggregation of high-level features. The GRU updates a hidden state $\mathbf{h}_t \in \mathbb{R}^{256}$ and outputs a temporal feature vector \mathbf{g}_t :

$$\mathbf{g}_t, \mathbf{h}_t = \text{GRU}(\mathbf{e}_t, \mathbf{h}_{t-1}), \quad (3)$$

where \mathbf{g}_t summarizes recent spatio-temporal context relevant for anomaly detection.

During training, sequences are unrolled for $T = 50$ steps with zero initialization; at inference, the hidden state is propagated online, with sensitivity to distant history decaying rapidly due to gating.

3) *Latent Bottleneck & Probabilistic Decoder*: To mitigate the risk of convergence to a trivial identity mapping, a known pathology in over-parameterized autoencoders [26], we adopt a denoising strategy coupled with a latent information bottleneck. During training, nominal observations are corrupted with additive Gaussian noise ($\sigma_{\text{noise}} = 0.01$). This forces the network to learn robust feature extractors rather than simply memorizing the input.

The recurrent features $\mathbf{g}_t \in \mathbb{R}^{256}$ are projected to a latent vector $\mathbf{z}_t \in \mathbb{R}^{d_{\text{latent}}}$ with $d_{\text{latent}} = 192$:

$$\mathbf{z}_t = \sigma(\text{LN}(\mathbf{W}_p \mathbf{g}_t + \mathbf{b}_p)). \quad (4)$$

Although this latent dimension exceeds the raw observation

space ($d_{\text{obs}} \approx 140$), it represents a moderate reduction from the recurrent feature space and was selected empirically as a stable operating point. Ablation results in Table II show that moderate compression outperforms more aggressive reductions.

To model heteroscedastic aleatoric uncertainty, we employ a probabilistic decoder g_θ that parametrizes a diagonal Gaussian distribution over the reconstruction:

$$[\mu_t, \log \sigma_t^2] = g_\theta(\mathbf{z}_t). \quad (5)$$

The model is trained end-to-end by maximizing the corresponding Gaussian likelihood of nominal observations, allowing reconstruction errors to be adaptively weighted by predicted uncertainty and thus down-weighting dimensions with higher intrinsic variability. The full loss expression is provided in the Supplementary Material. Optimization uses AdamW ($\alpha = 10^{-3}$, $B = 256$) with a OneCycleLR schedule over 100 epochs.

C. Hybrid Inference & Anomaly Detection

During inference, we employ a hybrid detection strategy combining deep contextual anomaly scoring (RAPT) with a deterministic range-based baseline. This design provides coverage for both learned contextual deviations and deterministic state-space constraint violations, ensuring a hard safety envelope independent of model uncertainty.

1) *NLL Calibration & Sim-to-Real Adaptation*: A key challenge transferring anomaly detectors to real hardware is the inevitable **Sim-to-Real gap** caused by differences in sensor noise, friction, and actuation latency. If unaccounted for, this static domain shift would lead to persistent false positives

when using simulation-derived thresholds. We therefore normalize the anomaly signal through a brief calibration phase in the target domain.

Let $\ell_{t,i}$ denote the per-dimension negative log-likelihood (NLL). During calibration, the expert policy is executed under nominal conditions for T_{cal} seconds, and the maximum observed residuals are recorded:

$$\tau_i^{\max} = \max_{t \in T_{\text{cal}}} \ell_{t,i}, \quad \tau_{\text{global}} = \max_{t \in T_{\text{cal}}} \left(\frac{1}{d_{\text{obs}}} \sum_{j=1}^{d_{\text{obs}}} \ell_{t,j} \right). \quad (6)$$

To maintain sensitivity to dynamic anomalies while suppressing false positives, we define thresholds using a *max-plus- $k\sigma$* rule. This choice is motivated by the heavy-tailed nature of many proprioceptive signals (e.g., joint velocities), for which high-percentile thresholds across hundreds of dimensions lead to excessive false positives in practice. In contrast, treating rare but benign calibration spikes as nominal yields more robust behavior under deployment noise.

We distinguish between *local* (per-dimension) and *global* (mean) deviations. Under nominal execution, the global mean NLL is empirically well-approximated by a Gaussian, consistent with aggregation effects across dimensions, and we therefore apply a tighter bound ($k = 3$) on the mean. In contrast, per-dimension thresholding operates in a multiple-comparisons regime and is used as a conservative safeguard against localized failures; accordingly, we apply a looser bound ($k = 5$) to individual dimensions:

$$\begin{aligned} \text{Gate}_{1,2}(\mathbf{o}_t) = & (\exists i : \ell_{t,i} > \tau_i^{\max} + 5\sigma_i) \\ & \vee (\bar{\ell}_t > \tau_{\text{global}} + 3\sigma_{\text{global}}). \end{aligned} \quad (7)$$

Here, σ denotes the standard deviation computed over the calibration set. This calibration removes static domain bias while preserving sensitivity to emerging failures.

2) *Bounding-Box Range Detector*: In parallel, we employ a simple range-based detector (Gate 3) that flags observations outside a calibrated hyper-rectangle. Bounds are estimated from nominal data and expanded by a margin δ :

$$\text{Gate}_3(\mathbf{o}_t) = \mathbf{o}_t \notin [\mathbf{o}^{\min} - \delta\Delta\mathbf{o}, \mathbf{o}^{\max} + \delta\Delta\mathbf{o}], \quad (8)$$

where $\Delta\mathbf{o} = \mathbf{o}^{\max} - \mathbf{o}^{\min}$ and $\delta = 0.05$ in simulation (0.2 on hardware).

The two detectors are complementary: RAPT captures contextual and temporally inconsistent behavior, while the range detector identifies explicit state-space constraint violations. The final anomaly decision is the logical OR of all gates.

D. Automated Root-Cause Analysis

Detecting an anomaly is necessary for safety, but identifying its cause is critical for debugging the Sim-to-Real gap and incident analysis. A binary flag does not explain whether a failure is due to terrain irregularities, sensor noise, or actuator degradation. We address this by introducing a two-stage diagnostic pipeline: 1) Gradient-based feature attribution to localize the fault, and 2) Semantic classification using a Large Language Model (LLM).

1) *Temporal Saliency via Backpropagation Through Time*: Given the recurrent nature of our architecture, a detected anomaly at time t is often the consequence of latent deviations accumulating over the recent history. To capture these temporal causal dependencies, we extend *Integrated Gradients* (IG) using Backpropagation Through Time (BPTT).

We define the input as a trajectory tensor $\mathbf{X}_t \in \mathbb{R}^{H \times d_{\text{obs}}}$ representing the window of $H = 200$ timesteps leading up to the failure: $\mathbf{X}_t = [\mathbf{o}_{t-H}, \dots, \mathbf{o}_t]$. Let $F(\mathbf{X}_t; \mathbf{h}_{t-H-1})$ denote the reconstruction Negative Log-Likelihood (NLL) at the final timestep t , conditioned on the hidden state \mathbf{h}_{t-H-1} preceding the window.

Crucially, by computing gradients with respect to the NLL rather than standard Mean Squared Error (MSE), the attribution scores are naturally weighted by the inverse variance ($\sigma_{t,i}^{-2}$). This ensures that deviations in highly uncertain (noisy) dimensions are down-weighted, focusing the saliency map on violations of high-confidence dynamic constraints.

Unlike standard saliency methods that attribute loss only to the current input, we compute temporal attributions over a history window. We compute temporal saliency using Integrated Gradients through time, attributing RAPT’s predictive deviation to individual features across a sliding history window. This yields a spatio-temporal attribution map that highlights which observations at which past timesteps contribute most strongly to the detected anomaly. Implementation details, including the baseline trajectory and integration procedure, are provided in the Supplementary Material.

Because F depends on a recurrent GRU, gradients propagate through the hidden state from τ to t , allowing the method to identify when a sensor or actuator begins to drift, even if the peak anomaly score occurs several timesteps later. This produces a spatio-temporal attribution heatmap over observations and time, enabling operators to distinguish sudden shocks (localized saliency near detection) from gradual degradation (diffuse saliency across the history window).

For visualization, we extract the most salient features at the time of detection and plot their temporal saliency over a fixed window preceding the anomaly (see Fig. 3); full plotting details are provided in the Supplementary Material.

2) *LLM-Based Root Cause Analysis*: While spatio-temporal saliency localizes *when* and *where* anomalous behavior emerges, it does not directly provide a semantic explanation of *why*. To assist post-hoc interpretation, we employ a large multi-modal language model (LLM) to map structured diagnostic evidence to a likely failure category.

The LLM is provided with a composite prompt containing: (i) the temporal saliency matrix derived via BPTT-integrated gradients; (ii) task context such as commanded velocities (for locomotion); (iii) kinematic state trajectories over the pre-failure window; and (iv) when available, an optional time-synchronized external camera key-frame. This design grounds the LLM’s reasoning in quantitative signals rather than raw text.

The model performs zero-shot classification over a pre-defined set of failure categories (Table I, Supplementary),

producing a semantic hypothesis intended to support operator diagnosis rather than replace it. Importantly, the LLM’s output is conditioned on statistically meaningful saliency patterns, enabling it to rule out implausible causes (e.g., terrain effects when attribution is isolated to upper-body sensors).

We emphasize that this component is designed as an assistive diagnostic tool. While validated on a subset of real-world failure modes, ambiguity remains in certain cases, particularly for closely related physical phenomena. We therefore treat LLM-based diagnosis as complementary to, rather than a substitute for, human judgment.

3) *Safety Responses*: Upon anomaly detection, RAPT triggers pre-defined safety responses selected by the operator based on task context. In our experiments, these included switching to a high-damping mode for controlled falling, halting motion and transitioning to a fixed standing posture, or commanding a backward step during collision scenarios. These responses are not autonomously synthesized by RAPT; rather, the system provides a reliable and timely trigger for human-specified safety behaviors. This design separates detection from control, allowing RAPT to be integrated with existing safety policies without modifying the underlying controller.

IV. EXPERIMENTAL SETUP

A. Tasks and Policies

We evaluate RAPT on four humanoid control tasks using the Unitree G1 (29 DoF): velocity-tracking locomotion, motion mimicry (Dance102, Gangnam), and ballistic throwing. Locomotion and mimicry tasks follow the `unitree_rl_lab` benchmark [25], while throwing is defined following [16]. For each task, five expert policies are trained using GCR-PPO [15] with different random seeds.

B. Simulation Protocol

We conduct large-scale OOD evaluation in NVIDIA Isaac Lab using $N_{env} = 4096$ parallel environments per task. Each evaluation run uses a 50/50 split: half of the environments execute nominal policies (false-positive evaluation), while the remaining half are subjected to controlled OOD perturbations (true-positive evaluation). A brief nominal calibration episode precedes testing to establish detection thresholds.

We inject 15 OOD categories spanning sensor faults, physics perturbations, and software/communication errors (details in Supplementary). This protocol enables statistically stable estimation of detection accuracy and false-positive behavior under realistic deployment conditions.

C. Baselines

We compare RAPT against representative state-of-the-art anomaly detectors: PatchAD [27], LSTM-VAE [21], Deep SVDD [23], and Isolation Forest [13]. All baselines are trained on identical nominal data and evaluated on the same logs.

Where source code was unavailable, we re-implemented methods following the original specifications. Hyperparameters were selected to ensure stable training under a 50Hz control regime and comparable computational budgets. Full implementation details are provided in the Supplementary Material.

D. Real-World Deployment

We deploy RAPT on a Unitree G1 humanoid at 50Hz. Upon anomaly detection, the system triggers predefined safety responses (e.g., halting motion or transitioning to a stable pose), ensuring safe operation during testing.

Real-world experiments include nominal trials and diverse perturbations such as external pushes, deformable terrain, payload attachment, footwear changes, and obstacles. We obtained a total of 24 OOD trials across tasks. All proprioceptive data and RAPT outputs are logged, and baselines are evaluated offline on identical trajectories.

E. Evaluation Metrics

In simulation, we report AUROC and True Positive Rate (TPR) at a fixed episodic False Positive Rate (FPR) of 0.5%, reflecting strict safety requirements in real-world deployment. We report inference runtime for each method, measured per environment and averaged across tasks, reflecting suitability for real-time deployment. Because all detectors operate at the same control frequency (50 Hz), detection latency is primarily determined by the anomaly scoring dynamics rather than raw inference speed. Category-specific detection delay statistics are therefore reported in the supplementary material.

For real-world diagnosis, we report True Positive and False Positive Rates of root-cause classification over labeled trials. Given the limited number of real-world experiments, these results are interpreted as indicative rather than exhaustive.

V. RESULTS

We structured our evaluation to answer three primary research questions:

- 1) **Detection Accuracy:** Does RAPT outperform state-of-the-art baselines in detection accuracy across a comprehensive suite of out-of-distribution (OOD) scenarios in simulation?
- 2) **Real-World Generalization:** Can RAPT generalize to physical hardware, maintaining sensitivity to real-world anomalies while remaining robust to the inevitable Sim-to-Real domain shift?
- 3) **Interpretability:** Can our gradient-based diagnostic pipeline correctly identify the semantic root cause of a failure?

A. Simulation Benchmarks

We evaluate anomaly detection performance in simulation following the protocol described in Section IV-B. Results are summarized using inference latency, AUROC, and Safety Score (TPR @ 0.5% FPR), as defined in the Experimental Setup.

Performance Analysis: As shown in Table I, RAPT attains the highest Safety Score and AUROC across all evaluated tasks while maintaining low inference latency (1.63 ms, < 10% of the 20 ms control budget). Compared to the strongest baseline (LSTM-VAE), RAPT achieves a +0.34 absolute improvement in Safety Score at the fixed false-positive operating point.

TABLE I: **Safety & Performance Comparison.** Safety Score (TPR @ 0.5% FPR) reported per task, with aggregate AUROC. RAPT attains the highest values on both metrics across all tasks. Model Only and Hybrid denote performance without and with the Range Detector, respectively. Results averaged over 5 seeds (\pm std). * indicates RAPT trained with a forward dynamics objective; all others use reconstruction.

Method	Global Metrics		Safety Score (TPR @ 0.5% FPR) by Task ↑				Ablation	
	Latency	Avg AUROC	Throwing	Velocity	Mimic (Dance)	Mimic (Gangnam)	Model Only	Hybrid
Isolation Forest	4.32 ms	0.69	0.24 \pm 0.04	0.34 \pm 0.03	0.42 \pm 0.01	0.38 \pm 0.00	0.18	0.34
PatchAD	11.45 ms	0.73	0.14 \pm 0.01	0.16 \pm 0.03	0.17 \pm 0.04	0.16 \pm 0.03	0.18	0.16
Deep SVDD	0.45 ms	0.67	0.29 \pm 0.03	0.31 \pm 0.10	0.41 \pm 0.01	0.37 \pm 0.01	0.14	0.34
LSTM-VAE	1.77 ms	0.77	0.30 \pm 0.02	0.36 \pm 0.02	0.44 \pm 0.01	0.42 \pm 0.01	0.32	0.38
Ours (RAPT)	1.63 ms	0.92	0.72 \pm 0.05	0.74* \pm 0.02	0.67 \pm 0.08	0.75 \pm 0.02	0.75	0.72

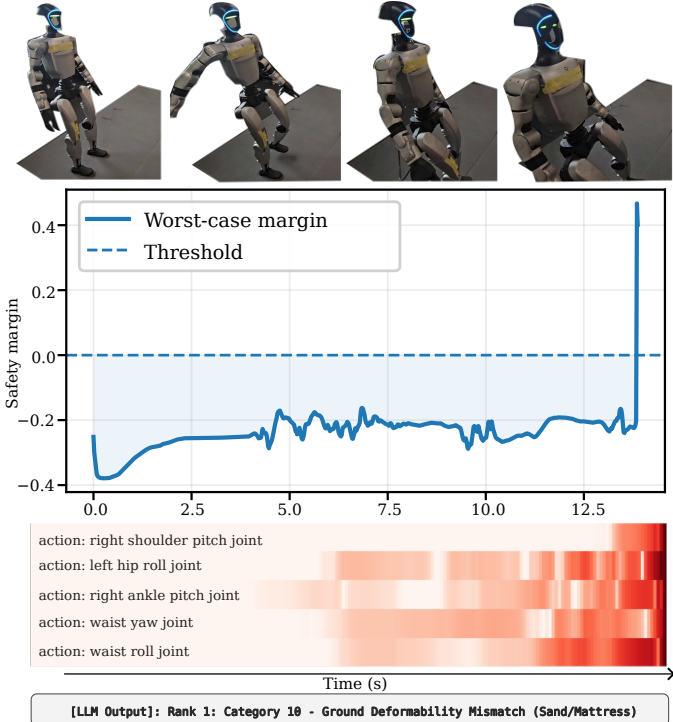


Fig. 3: **RAPT on a real-world anomaly.** Top: stumble on deformable ground during a low-magnitude walking command. Second: NLL margin to threshold, spiking at failure. Third: Top-5 temporal saliency heatmap. Bottom: LLM-based diagnosis from proprioceptive saliency and joint states.

Notably, the relative performance gap between RAPT and prior methods is more pronounced for Safety Score than AUROC. This suggests that several baselines achieve reasonable threshold-independent separability, but struggle with sensitivity when false positives are tightly constrained. We attribute this to overlap between in-distribution and out-of-distribution tails, which degrades precision at low false-positive rates.

Hybrid vs. Model-Only Detection: To ensure fair comparison, all methods were evaluated both with and without the auxiliary Range Detector. As shown in the *Model Only* and *Hybrid* columns of Table I, shallow baselines (e.g., Isolation Forest, Deep SVDD) rely heavily on explicit range checks, exhibiting reduced performance when evaluated in isolation. In contrast, RAPT remains robust without the range detector

TABLE II: **Taguchi L12 Ablation Analysis.** Feature importance rankings (via Random Forest) and marginal mean Safety Scores (TPR @ 0.5% FPR). Δ TPR demonstrates the average TPR improvement for setting A over setting B.

Factor	Imp.	Setting A	Setting B	Best	Δ TPR
Detection Logic (Inference)	35.4%	Max 0.543	Mean 0.400	Max	+0.143
Uncertainty (Training)	20.8%	Probabilistic 0.534	Deterministic 0.431	Prob.	+0.103
Dynamics (Recurrence)	18.5%	Temporal 0.520	Static 0.435	Temp.	+0.085
Training Target (Objective)	7.3%	Dynamics 0.491	Reconstruction 0.486	Dyn.	+0.005
Gradient Flow (Residual Conn.)	6.7%	Residual 0.513	None 0.468	Res.	+0.045
Compression	6.1%	Low (25%) 0.530	High (75%) 0.452	25%	+0.078
Reconstruction Type	5.2%	Bottleneck 0.512	Masking 0.461	Bottle.	+0.052

(0.75 vs. 0.72 Safety Score), indicating that it internalizes much of the valid state manifold structure. The small drop in the hybrid setting is attributable to additional false positives introduced by conservative range thresholds.

B. Ablation Studies

We analyze the contribution of key architectural and algorithmic design choices using a Taguchi L12 orthogonal array ablation over 48 models (Table II). Feature importance is computed via a Random Forest regressor, and marginal mean Safety Scores are reported at a fixed false-positive rate.

Inference Logic is the dominant factor (35.4% importance): per-dimension aggregation using the maximum anomaly score improves Safety Score by +14.3% over mean aggregation. This suggests that, under reconstruction/NLL scoring, deviations are often concentrated in a subset of observation dimensions; mean aggregation can dilute these signals even when the underlying behavior is substantially off-nominal.

Probabilistic modeling (NLL) improves robustness under heteroscedastic noise (+10.3%) compared to deterministic reconstruction error. Architectural choices further contribute, including **Temporal Recurrence** (+8.5%), **Residual Connections** (+4.5%), and **Low Latent Compression** (+7.8%).

The **Training Target** exhibits task dependence: command-conditional walking benefits from a forward dynamics ob-

jective, while manipulation and mimicry tasks favor direct reconstruction. These results motivate the final design choices used in RAPT.

C. Real-World Deployment

We evaluate RAPT on physical hardware using the deployment protocol described in Section IV-D. A brief nominal execution is used to calibrate detection thresholds, resulting in zero false positives during nominal operation.

We then evaluate the system on 24 anomalous trials spanning multiple physical perturbation categories. Given the limited and safety-constrained nature of real-world testing, these results are intended as indicative rather than exhaustive.

As shown in Table III, the Hybrid RAPT configuration achieves the highest recall (75%), detecting 18 out of 24 anomalous runs. Evaluating individual components highlights their complementary roles:

- **RAPT (67% recall):** Sensitive to dynamic interaction faults that do not violate explicit state bounds, including wall contacts and non-catastrophic stumbles.
- **Range Detector (62% recall):** Provides a conservative safety guarantee by flagging explicit state-space violations, such as large gravity deviations or joint limit exceedances.
- **Baseline LSTM-VAE (50% recall):** Exhibits reduced sensitivity in the real-world domain, particularly for anomalies that do not immediately lead to failure.

Beyond quantitative detection, RAPT proved useful as a deployment verification tool. During integration, it flagged silent configuration errors—such as under-tuned wrist PD gains—that were not captured by range checks alone. This highlights its utility for identifying subtle sim-to-real inconsistencies that degrade performance without triggering hard safety limits.

D. Automated Root-Cause Diagnosis

We evaluate the diagnostic pipeline on 16 real-world failure logs for which complete diagnostic data were available following successful anomaly detection by RAPT (Hybrid), classifying each into one of 21 predefined failure categories (see Supplementary Material, Table II). Results are reported for two configurations: Proprioceptive Only and Multi-Modal (with a single time-synchronized visual keyframe).

As shown in Table IV, the Multi-Modal configuration improves both Top-1 and Top-3 accuracy relative to the proprioceptive-only baseline. Visual context enables disambiguation between external disturbances and internal system faults (e.g., obstacle vs. motor dynamics mismatch).

From an operational perspective, narrowing failures to the correct subsystem (e.g., leg actuation vs. perception) can substantially reduce post-incident debugging time. In practice, we found the diagnostic pipeline particularly useful for identifying silent sim-to-real discrepancies, such as mismatched PD gains or implementation-level inconsistencies in state estimation.

TABLE III: **Anomaly Detection Performance Comparison on Real G1 Humanoid.** Results over $N = 27$ trials (24 anomalous, 3 nominal). We report true/false positives, precision, recall, and F1 for baseline methods and RAPT variants.

Method	TP ↑	TN ↑	FN ↓	Prec.	Rec.	F1
SVDD	6	3	18	1.000	0.250	0.400
Isolation Forest	7	3	17	1.000	0.291	0.451
PatchAD	10	3	14	1.000	0.416	0.588
LSTM	12	3	12	1.000	0.500	0.667
Range Detector	15	3	9	1.000	0.625	0.769
RAPT (Ours)	16	3	8	1.000	0.667	0.800
RAPT + Range (Hybrid)	18	3	6	1.000	0.750	0.857

TABLE IV: **Root-Cause Analysis (RCA) Accuracy across 16 Real-World Failure Scenarios.** We report Top-1 and Top-3 classification accuracy using proprioceptive saliency alone (Prop.) and with an additional visual keyframe (Prop. + Visual).

Method	Top-1 Accuracy		Top-3 Accuracy	
	Count	Percentage (%)	Count	Percentage (%)
Proprioceptive Only (RAPT)	12 / 16	75%	14 / 16	87.5%
RAPT + Visual Key-frame	14 / 16	87.5%	16 / 16	100%
<i>Improvement</i>	2 / 16	12.5%	2 / 16	12.5%

VI. DISCUSSION AND CONCLUSION

In this paper, we presented RAPT, a lightweight, self-supervised system for detecting and diagnosing out-of-distribution (OOD) behavior during sim-to-real deployment of humanoid robots. The method addressed the risk of silent policy failure by learning a probabilistic spatio-temporal model of nominal operation and using calibrated reconstruction likelihoods to detect deviations at high frequency. Through extensive simulation and real-world deployment, we demonstrated that RAPT outperformed existing baselines at a fixed low false-positive rate while remaining suitable for real-time use. We further showed that reconstruction-based saliency enables automated, semantically meaningful root-cause diagnosis using only proprioceptive data.

The results indicate that treating reconstruction error as a continuous measure of sim-to-real mismatch, rather than a binary failure signal, provides practical value beyond safety triggering alone. In simulation, this formulation enabled sensitivity to subtle dynamic deviations under strict false-positive constraints. In real-world deployment, RAPT proved useful not only for triggering appropriate safety responses but also for verifying sim-to-real consistency and diagnosing silent configuration or modeling errors that would not violate simple range-based checks. This perspective complements existing sim-to-real approaches such as domain randomization and system identification by providing a deployment-time signal of domain mismatch.

The proposed approach has several limitations. Real-world quantitative evaluation was limited by hardware availability and operational constraints, resulting in a modest number of trials and a restricted subset of OOD events; all experiments were conducted on a single humanoid platform over short-term deployments. In addition, the calibration strategy is

intentionally simple and does not explicitly model the nominal distribution of each observation dimension, which may lead to false negatives in cases where more expressive uncertainty modeling could better separate subtle anomalies. Addressing these limitations is an important direction for future work, including improving detection at even lower false-positive rates and using RAPT as a domain-measurement signal for downstream decision-making, such as policy switching across distinct distributional regimes.

REFERENCES

- [1] Mohammed Alshiekh, Roderick Bloem, Rüdiger Ehlers, Bettina Könighofer, Scott Niekum, and Ufuk Topcu. Safe reinforcement learning via shielding. In *Proceedings of the AAAI Conference on Artificial Intelligence*, volume 32, 2018.
- [2] Felix Berkenkamp, Matteo Turchetta, Angela Schoellig, and Andreas Krause. Safe model-based reinforcement learning with stability guarantees. In *Advances in neural information processing systems*, volume 30, 2017.
- [3] Lukas Brunke, Melissa Greeff, Adam W Hall, Zhaocong Yuan, Siqi Zhou, Jacopo Panerati, and Angela P Schoellig. Safe learning in robotics: From learning-based control to safe reinforcement learning. *Annual Review of Control, Robotics, and Autonomous Systems*, 5:411–444, 2022.
- [4] Richard Cheng, Gábor Orosz, Richard M Murray, and Joel W Burdick. End-to-end safe reinforcement learning through barrier functions for safety-critical continuous control tasks. In *Proceedings of the AAAI Conference on Artificial Intelligence*, volume 33, pages 3387–3395, 2019.
- [5] Yinlam Chow, Ofir Nachum, Aleksandra Faust, Edgar Duenez-Guzman, and Mohammad Ghavamzadeh. Lyapunov-based safe policy optimization for continuous control. *arXiv preprint arXiv:1901.10031*, 2019.
- [6] Mohamed Elnoor, Adarsh Jagan Sathyamoorthy, Kasun Weerakoon, and Dinesh Manocha. Pronav: Proprioceptive traversability estimation for legged robot navigation in outdoor environments. *IEEE Robotics and Automation Letters*, 9(8):7190–7197, 2024.
- [7] David Ha and Jürgen Schmidhuber. Recurrent world models facilitate policy evolution. *Advances in neural information processing systems*, 31, 2018.
- [8] Tom Haider, Karsten Roscher, Felipe Schmoeller da Roza, and Stephan Günnemann. Out-of-distribution detection for reinforcement learning agents with probabilistic dynamics models. In *Proceedings of the 2023 International Conference on Autonomous Agents and Multiagent Systems*, pages 851–859, 2023.
- [9] Tom Haider, Karsten Roscher, Benjamin Herd, Felipe Schmoeller Roza, and Simon Burton. Can you trust your agent? the effect of out-of-distribution detection on the safety of reinforcement learning systems. In *Proceedings of the 39th ACM/SIGAPP Symposium on Applied Computing*, pages 1569–1578, 2024.
- [10] Rachel Hornung, Holger Urbanek, Julian Klodmann, Christian Osendorfer, and Patrick Van Der Smagt. Model-free robot anomaly detection. In *2014 IEEE/RSJ International Conference on Intelligent Robots and Systems*, pages 3676–3683. IEEE, 2014.
- [11] Advait Jain, Marc D Killpack, Aaron Edsinger, and Charles C Kemp. Reaching in clutter with whole-arm tactile sensing. *The International Journal of Robotics Research*, 32(4):458–482, 2013.
- [12] Jingyao Li, Pengguang Chen, Zexin He, Shaozuo Yu, Shu Liu, and Jiaya Jia. Rethinking out-of-distribution (ood) detection: Masked image modeling is all you need. In *Proceedings of the IEEE/CVF conference on computer vision and pattern recognition*, pages 11578–11589, 2023.
- [13] Fei Tony Liu, Kai Ming Ting, and Zhi-Hua Zhou. Isolation forest. In *2008 eighth ieee international conference on data mining*, pages 413–422. IEEE, 2008.
- [14] Aaqib Parvez Mohammed and Matias Valdenegro-Toro. Benchmark for out-of-distribution detection in deep reinforcement learning. *arXiv preprint arXiv:2112.02694*, 2021.
- [15] Humphrey Munn, Brendan Tidd, Peter Böhm, Marcus Gallagher, and David Howard. Scalable multi-objective robot reinforcement learning through gradient conflict resolution. *arXiv:2509.14816*, 2025.
- [16] Humphrey Munn, Brendan Tidd, Peter Böhm, Marcus Gallagher, and David Howard. Whole-body dynamic throwing with legged manipulators. In *Proceedings of the 27th Australasian Conference on Robotics and Automation (ACRA)*, Perth, Australia, December 2025. Available at [arXiv:2410.05681](https://arxiv.org/abs/2410.05681).
- [17] Anusha Nagabandi, Kurt Konolige, Sergey Levine, and Vikash Kumar. Deep dynamics models for learning dexterous manipulation. In *Conference on Robot Learning (CoRL)*, pages 1101–1112. PMLR, 2020.
- [18] Eric Nalisnick, Akihiro Matsukawa, Yee Whye Teh, Dilan Gorur, and Balaji Lakshminarayanan. Do deep generative models know what they don’t know? *arXiv preprint arXiv:1810.09136*, 2018.
- [19] Linas Nasvytis, Kai Sandbrink, Jakob Foerster, Tim Franzmeyer, and Christian Schroeder de Witt. Rethinking out-of-distribution detection for reinforcement learning: Advancing methods for evaluation and detection. *arXiv preprint arXiv:2404.07099*, 2024.
- [20] Masashi Okada and Tadahiro Taniguchi. Variational inference mpc for bayesian model-based reinforcement learning. In *Conference on robot learning*, pages 258–272. PMLR, 2020.
- [21] Daehyung Park, Yuuna Hoshi, and Charles C Kemp. A multimodal anomaly detector for robot-assisted feeding using an lstm-based variational autoencoder. *IEEE Robotics and Automation Letters*, 3(3):1544–1551, 2018.
- [22] Mohit Prashant, Arvind Easwaran, Suman Das, and Michael Yuhas. Guaranteeing out-of-distribution detection in deep rl via transition estimation. In *Proceedings*

of the AAAI Conference on Artificial Intelligence, volume 39, pages 12452–12460, 2025.

- [23] Lukas Ruff, Robert Vandermeulen, Nico Goernitz, Lucas Deecke, Shoaib Ahmed Siddiqui, Alexander Binder, Emmanuel Müller, and Marius Kloft. Deep one-class classification. In *International conference on machine learning*, pages 4393–4402. PMLR, 2018.
- [24] Abdellah Zakaria Sellam, Ilyes Benaissa, Abdelmalik Taleb-Ahmed, Luigi Patrono, and Cosimo Distante. Mamba adaptive anomaly transformer with association discrepancy for time series. *arXiv preprint arXiv:2502.07858*, 2025.
- [25] Unitree Robotics. *unitree_rl_lab*: Reinforcement learning implementation for unitree robots based on isaaclab. https://github.com/unitreerobotics/unitree_rl_lab, 2024.
- [26] Pascal Vincent, Hugo Larochelle, Yoshua Bengio, and Pierre-Antoine Manzagol. Extracting and composing robust features with denoising autoencoders. In *Proceedings of the 25th International Conference on Machine Learning*, pages 1096–1103, 2008.
- [27] Zhijie Zhong, Zhiwen Yu, Yiyuan Yang, Weizheng Wang, Kaixiang Yang, and CL Philip Chen. Patchad: A lightweight patch-based mlp-mixer for time series anomaly detection. *IEEE Transactions on Big Data*, 2025.